Original Research

# Shifted hub regions in the brain network of rat neuropathic pain model after electroacupuncture therapy

Jiajia Wu[1], Shuai Wang[2], Yechen Lu[3], Mouxiong Zheng[1,4], Xuyun Hua[1,4] and Jianguang Xu[1,3,5,*]

[1]*Center of Rehabilitation Medicine, Yueyang Hospital of Integrated Traditional Chinese and Western Medicine, Shanghai University of Traditional Chinese Medicine, Shanghai, 200437, P. R. China*

[2]*Department of Rehabilitation Medicine, Ordos Central Hospital, Ordos, 017000, P. R. China*

[3]*School of Rehabilitation Science, Shanghai University of Traditional Chinese Medicine, 201203, Shanghai, P. R. China*

[4]*Department of Trauma and Orthopedics, Yueyang Hospital of Integrated Traditional Chinese and Western Medicine, Shanghai University of Traditional Chinese Medicine, Shanghai, 200437, P. R. China*

[5]*Department of Hand Surgery, Huashan Hospital, Fudan University, Shanghai, 200041, P. R. China*

*Correspondence: jianguangxu@fudan.edu.cn (Jianguang Xu)

Electroacupuncture has been considered an effective neurorehabilitative approach to relieve neuropathic pain originating in the central nervous system. However, the neural mechanism underlying the effect of electroacupuncture on pain-relief remains largely unknown. The objective of this study was to investigate the alteration of hub configurations of brain networks caused by the sustained impact of electroacupuncture on a clinically relevant animal model of neuropathic pain. Rats were divided into four groups: normal, model, electroacupuncture, and sham-electroacupuncture. Rats of the last three groups received complete brachial plexus avulsion to evoke neuropathic pain. Electroacupuncture was conducted continuously for three months on the electroacupuncture group, while the sham intervention was performed on the sham-electroacupuncture group. Mechanical withdrawal thresholds were evaluated at the end of the first and third month of intervention. Graph theoretical network analysis compared the regional topological parameters and explored hub configurations of brain networks by longitudinal resting-state fMRI. Three-months electroacupuncture showed a significant pain-relief effect. Not the spatial distribution of hubs, but the hubness distribution showed a significant difference among groups after a three-month intervention. The proportion of more highly connected hub regions was significantly higher in the model rats than the normal rats, while that of the electroacupuncture group was considerably lower than the model group. Additionally, regional parameter changes showed a very similar distribution of hub proportions. It was concluded that long-term electroacupuncture might restore an adaptive equilibrium to a disrupted network and suppress maladaptive plastic changes that follow neuropathic pain. This may provide an important avenue for future strategies appropriate for therapeutic interventions.

## Keywords

## 1. Introduction

Acupuncture, a necessary complementary and alternative therapy treatment, has been shown to provide a practical neurorehabilitative approach to the relief of neuropathic pain without causing dependency. The mechanism of pain relief has been proposed to be associated with the release of neurotransmitters, such as endorphins (Han, 2004; Pomeranz, 1996). Electroacupuncture (EA) is an acupuncture-based technique where a small electric current is transmitted between pairs of acupuncture needles. EA shows a positive effect on pain relief by activating a range of bioactive chemicals that contributed to peripheral, spinal, and supraspinal actions (Zhang et al., 2014). Given that maladaptive brain, plasticity is associated with the occurrence and recovery of neuropathic pain (Dhond et al., 2007), therapeutic strategies for pain-relief characteristically target this central mechanism.

The vertebrate brain is a complex network of interacting regions. The elucidation of functional features of such a brain network has the potential to improve understanding of how EA might help relieve pain. Highly connected regions of the whole brain or hubs have been extensively explored as they are critical for brain function (Nijhuis et al., 2013; van den Heuvel and Sporns, 2011). It has been demonstrated that hub regions of normal brain networks shift, specifically following acupuncture (Liu et al., 2012). Furthermore, current reviews suggest that acupuncture could modulate both regional and extended spontaneous neural activities in the resting brain network (Dhond et al., 2008; Fang et al., 2009; Hui et al., 2005). This study focuses on the hub configurations of the whole-brain network. It shows how external EA intervention

interacts with internal regulatory processes by rearranging hub regions, an effect which might provide novel insight into the mechanisms involved in the relief of neuropathic pain by acupuncture (Dhond et al., 2008).

A clinically relevant neuropathic pain rat model of brachial plexus avulsion (BPA) was employed, long-term EA intervention performed, and stimulus-evoked pain responses following injury were monitored. In parallel, regional topological parameters were compared, and hub configurations of brain networks after EA treatment explored by longitudinal resting-state fMRI neuroimaging. The aim was to obtain a new perspective on central mechanisms underlying EA for pain relief, which might potentially be clinically applicable.

## 2. Materials and Methods

### 2.1 Animals

Fifty female Sprague-Dawley rats weighing 200-250 g were used in this study. Eight rats that underwent no further experimental procedures were randomly selected to provide a normal control (normal group). The remaining 42 rats were assigned to the model establishment. After surgery, rats were screened, and those presenting self-harm behavior were determined to have neuropathic pain syndrome. Twenty-four rats with neuropathic pain were randomly divided into three groups equal in number: model group, EA group, and sham-EA group. All protocols and procedures employed in this study followed animal care guidelines and were approved by the local committee.

### 2.2 Model establishment

BPA established an animal model of neuropathic pain following Wang et al. (2019). Surgical procedures were performed when adequate anesthesia (40 mg/kg sodium pentobarbital intraperitoneal injection) was achieved. Briefly, an approximate 4 cm incision was made along the dorsal midline using the C7 vertebra as a bone mark. To expose the nerve roots from C5 to T1, the lamina was removed from the right side of the vertebra (C4-T1) under an operating microscope (magnification × 10) through a posterior approach. After being dissociated, both dorsal and ventral rootlets from C5 to T1 were avulsed by a retractor. The same experienced operator performed all these procedures.

### 2.3 EA and sham-EA intervention

Before the intervention, a period of three to four weeks was left for the rats to recover from the surgery. A three-day adaption training was then applied to minimize anxiety for the rats. During the EA intervention, rats were held on a customized platform. In the present study, the parameters of EA were developed in accordance with both literature and the clinical experience of acupuncture experts. Additionally, previous studies have shown that EA on "Jiaji" points relieves some pain conditions, including persistent tissue injury (inflammation), nerve injury (neuropathy), cancer and visceral pain (Chen et al., 2018, 2013; Liu et al., 2016; Xu et al., 2010).

For EA intervention, acupuncture was delivered using four disposable, stainless steel needles (diameter 0.3 mm, length 13 mm, Huatuo, Suzhou, PRC) which were inserted into "Jiaji" on the left side (5 mm horizontally away from the 5th cervical vertebra to the 1st thoracic vertebra, depth 5 mm). EA was applied by an electrical stimulator (Huatuo SDZ-II, Suzhou Medical Appliance Fac-

tory, PRC) on two non-adjacent needles. The stimulator delivered dense disperse waves of 2/15 Hz at 1 mA (adjusted to the muscle twitch threshold) for 30 min/day. For sham-EA, four needles were inserted into the non-acupoints besides "Jiaji" on the left side. The intervention was performed five times per week for three months.

### 2.4 Mechanical withdrawal thresholds

Mechanical withdrawal threshold (MWT) tests were performed one month and three months post-intervention to assess changes in pain perception. The timeline of this study is shown in Fig. 1. In consideration of the peripheral sensitization mechanism associated with neuropathic pain, the pain threshold of bilateral intact hindpaws was utilized as the indicator of the overall pain threshold aroused by BPA (Rodriguesfilho et al., 2003). Prior study has consistently demonstrated that the MWT of bilateral hindpaws significantly decreases after BPA when compared with pre-modeling (Wang et al., 2019).

For MWT tests, rats were individually held in a transparent plastic box on an elevated mesh grid. After a 30-min acclimatization period, a linearly increasing mechanical force (0.6, 1.4, 2, 4, 6, 8, 10, and 15 g) was applied to the plantar surface of the hindpaw by use of Von Frey monofilaments (Stoelting, IL). A response was considered positive if a quick foot withdrawal response, flinching, or licking was observed. The MWT was determined as the lowest force that triggered a positive response to at least 2 out of 4 repeated stimuli (Chaplan et al., 1994).

### 2.5 fMRI data acquisition

Resting-state fMRI data were acquired on a 7T system (horizontal-bore animal MRI scanner, Bruker, Germany) at two-time points: at the end of the first and third months of EA intervention. The present study utilized a single transmit and surface receiving coil to receive the signal. Rats were anesthetized with isoflurane (4% initially for induction, 1.5%-2% for maintenance) and given necessary ventilator support during the scanning. Functional MR images were then acquired using an interleaved single-shot echo planar image (EPI) sequence with the same parameters as reported previously (Wu et al., 2018). Scanning parameters included: repetition time 3000 ms, echo time 20 ms, flip angle 90°, field of view $32 \times 32$ mm$^2$ and slice thickness 0.5 mm.

### 2.6 fMRI data preprocessing

Data were preprocessed by using an SPM8 toolbox (http://www.fil.ion.ucl.ac.uk/spm/) and Matlab version 2014a (www.mathworks.com) software platforms. After converting the raw Digital Imaging and Communications in Medicine (DICOM) data to Neuroimaging Informatics Technology Initiative (NIFTI) images, all images were rescaled by a factor of ten such that the image size approximated the scale of the human brain. This allowed the use of processing algorithms originally developed for human data (Moya et al., 2015; Wu et al., 2018). This procedure only changed the dimension information in the header file and required no interpolation of data. Additionally, none-brain tissue was stripped manually to facilitate image processing. Subsequently, acquired functional images were corrected for differences in slice scan time and spatially realigned with a six parameter (rigid body) transformation to remove movement artifacts. A transformation was then estimated from the mean image to a standard template (Schwarz et al., 2006) and applied to fMRI data for individual Montreal Neuro-
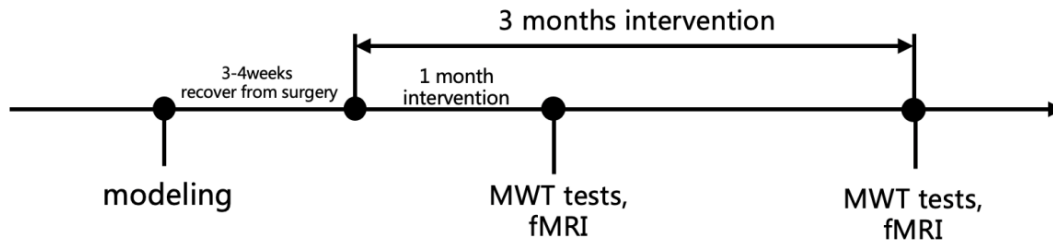
Figure 1. The timeline of the study. A period of three to four weeks was left for the rats to recover from the surgery before the intervention. Resting-state fMRI and mechanical withdrawal threshold (MWT) tests were conducted after one and three-months of intervention.

logical Institute normalization. Spatial smoothing was performed with a full-width half-maximum Gaussian kernel of twice as the voxel size. Subsequently, linear detrending and band-pass filtering (0.01-0.08 Hz) were performed. Finally, nuisance variables (blood oxygen level-dependent signal of the global brain, white matter, and cerebral spinal fluid and motion parameters) were further regressed out (Fox et al., 2009).

### 2.7 Functional Connectivity Matrix and Graph Construction

A functional connectivity matrix was constructed using a graph theoretical network analysis toolbox for imaging connectomics (GRETNA, http://www.nitrc.org/projects/gretna/) (Wang et al., 2015). Schwarz et al. (2006) were used to divide the whole brain into 96 regions, which were then considered as nodes of the brain networks. For each brain region, time series were acquired by averaging the time course across all voxels within each given region. Pearson's correlations between the mean time series of all node pairs were computed as the edges of a brain functional network. The result was a $96 \times 96$ symmetric correlation matrix for each rat, which was then converted into a binary matrix at a specified sparsity (Suo et al., 2015). Notably, the number of edges generated by this method divided by the maximum possible number of edges is referred to as the sparsity of the network. To obtain networks with the same number of edges, the sparsity range was set for each correlation matrix. This allowed prominent small-world properties in the brain networks to be observed (Watts and Strogatz, 1998). Accordingly, each absolute matrix was restricted at each sparsity level (a threshold range of 0.05 < sparsity < 0.45 with an interval of 0.01) to generate a set of undirected and unweighted binarized networks. Finally, graph theoretical network analysis was performed using GRETNA.

### 2.8 Topological analysis of brain networks
#### 2.8.1 Nodal properties

For brain networks, nodal properties can be measured by nodal degree, nodal efficiency, and betweenness centrality. A nodal degree is the number of links connected to a focal node (Sporns and Zwi, 2004). Nodal efficiency is a measure of local connectivity and calculated as the averaged reciprocal of the minimum path length between the given node and all other nodes (Achard and Bullmore, 2007). The betweenness centrality of a node quantifies the importance of a node within a network and is defined as the number of shortest paths between pairs of other nodes that pass through the given node (Freeman, 1977).

To further simplify the statistical analysis, an integrated nodal parameter ($S_{nod}$) was employed as a scalar value that summarized a topological characterization (Tian et al., 2011). $S_{nod}$ was calculated as the area under the curve of each nodal parameter over the sparsity range (Xu et al., 2014).

#### 2.8.2 Hub identification

To determine the hubs in the brain network, the normalized nodal parameter ($NS_{nod}$) was firstly computed (Xu et al., 2014):

$$NS_{nod}(i) = \frac{N \sum_{k=1}^{M} S_{nod}(i,k)}{\sum_{j=1}^{N} \sum_{k=1}^{M} S_{nod}(i,k)}$$

where Snod (i, k) is one of the three $S_{nod}$ (degree, nodal efficiency, and betweenness centrality) at node $i$ for the brain network of subject k, and N is the number of nodes (N = 96), and M is the number of subjects (M = 8).

Hubs, highly connected nodes in a network, were defined as the nodes any of the three normalized nodal parameters of which was at least one standard deviation (SD) greater than the average value. Hubs were determined corresponding to every group at each time point.

Additionally, hubs were determined according to the above formula and defined individually for each animal. And the node was identified to be the more highly connected hub region if any of its three nodal parameters was at least 2.5 SD greater than the average value. The proportion of these more highly connected hub regions of the hubs were then calculated for each brain network.

### 2.9 Statistical analysis

Statistical analysis was performed with Matlab software. Repeated measures analysis of variance was performed to analyze behavioral data. Post-hoc pairwise comparison was performed to identify significant between-group differences at each time point using a Bonferroni-Dunn test. A $P$-value < 0.05 was considered to indicate a significant difference between samples. The integrated regional network parameters were used for the Kruskal-Wallis test at each time point. If there was a significant overall difference among groups, further group comparison was performed by a nonparametric permutation test at each time point. $P < 0.05$ after false discovery rate (FDR) correction was considered significant. To determine whether there was a statistical difference in the proportions of more highly connected hub regions, the Friedman test was performed. Wilcoxon signed-rank tests were performed to assess
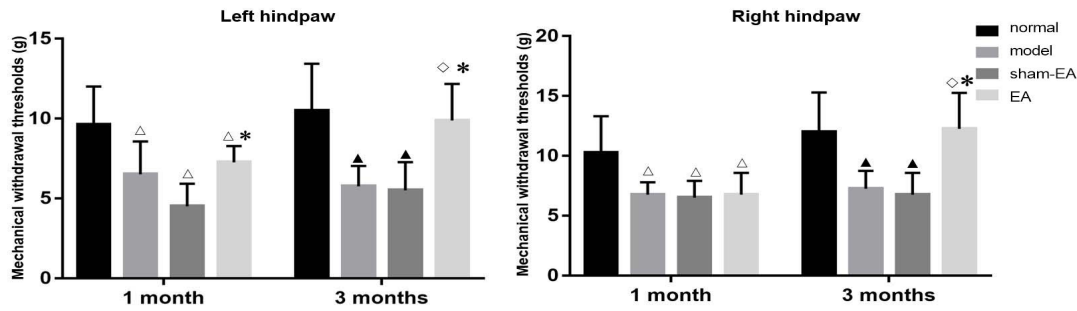
Figure 2. Mechanical withdrawal threshold of bilateral hindpaws of four groups after one and three-months of EA intervention. Data are expressed as mean $\pm$ standard error of the mean (SEM) for eight animals in each group. $\triangle$ $P < 0.05$, as compared to the normal group; $\blacktriangle P < 0.01$, as compared to the normal group; $\diamond P < 0.01$, as compared to the model group; $* P < 0.01$, as compared to the sham-EA group.

the difference between either two groups at the same time point. To compare the difference between two-time points in the same group, pairwise signed-rank tests were performed. The threshold for significance was set at $P < 0.05$.

## 3. Results

### 3.1 Mechanical withdrawal thresholds

A significant main effect for group comparisons was found for the mechanical withdrawal latency (MWL) of left hindpaws (F (3, 28) = 22.581, $P < 0.05$) and right hindpaw (F (3, 28) = 13.100, $P < 0.05$). After one month of EA intervention, MWL of bilateral hindpaws in the model, EA, and sham-EA groups were significantly lower than that of the normal group ($P < 0.05$). Alternatively, MWL of the left hindpaws in the EA group was significantly higher than that of the sham-EA group ($P < 0.01$). For MWL of right hindpaws, there was no significant difference among the model, sham-EA, and EA groups. After the three-months of EA intervention, MWLs of bilateral hindpaws in the model and sham-EA groups were both significantly lower than those of the normal group ($P < 0.01$), while no significant difference was found between the EA and normal groups for MWL in the left hindpaws. MWLs of bilateral hindpaws in the EA group were significantly higher than those in the model and sham-EA groups ($P < 0.01$) after three-months of EA intervention (Fig. 2).

### 3.2 Hub regions

Based on the nodal properties, hubs were defined in functional brain networks in each of the four groups of rats at each of the two tested time-points. The hubs identified in each group at each time point are given in Table 1 and mapped onto the rat brain surface for visualization (Fig. 3). Results showed a similar spatial distribution of hubs among the four groups. Hub regions were predominately located in the limbic system (such as entorhinal cortex, nucleus accumbens shell, piriform cortex, hippocampus, and hypothalamus), parietal lobes (motor cortex), midbrain (ventral tegmental area, mesencephalic region, superior colliculus, and substantia nigra), medial temporal lobe (olfactory tubercle, nucleus accumbens, diagonal band, and substantia innominata) and subcortical regions (ventral pallidum and thalamus).

### 3.3 Differences in the proportion of more highly connected hub regions

Significant differences in the proportion of more highly connected hub regions were found across all groups (Friedman's Chi-square 17.07, df 3 28, $P = 0.0079$). However, further analysis showed that after the one-month of EA intervention, there was no significant difference among the four groups. After three months of EA intervention, the proportion of more highly connected hub regions in the model group was significantly higher than that of the normal group ($P = 0.048$), while, conversely, the proportion of the EA group was substantially lower than that of the model group ($P = 0.049$). No statistical difference was found between the EA and normal groups or between the sham-EA and other groups (Fig. 4).

### 3.4 Differences in the integrated regional network parameters

In addition to the abovementioned network metrics, differences of the integrated regional network parameters were determined for each brain area (Table 2).

At the end of the first month of EA intervention, the right mesencephalic region exhibited a significantly higher degree for the model group than for the normal group, while the right mesencephalic region and left periaqueductal grey showed a substantially lower degree for the EA group as compared to the model group. Betweenness centrality of the left amygdala in the EA group was significantly lower than that in the normal group. Concerning nodal efficiency, no significant difference was found among the four groups of rats after one-month of EA intervention.

At the end of the third-month of EA intervention, betweenness centrality of right olfactory nuclei in the model group was significantly lower than that of the normal group, while betweenness centrality of the left anterior dorsal hippocampus and left pons in the model group was significantly higher than that of the normal group. When compared with the model group, the left anterior dorsal hippocampus exhibited a substantially lower degree of hubness in the EA group. Betweenness centrality of right olfactory nuclei and left amygdala in the EA group were significantly lower than that of the normal group. Only for the left anterior dorsal hippocampus was the nodal efficacy in the model group substantially higher than that of the normal group. The right lateral hy-

Wu et al.

Table 1. Hub regions of the functional neural networks of four groups after 1-month and 3-month intervention.

| group | hub regions | location | Multiple of SD | hub regions | location | Multiple of SD |
|---|---|---|---|---|---|---|
| | | | 1 month | | 3 months | |
| EA | L_ic | subcortical regions | 1.03 | R_Hippocampus_Ventral | | 1.02 |
| | L_Cortex_Piriform | limbic system | 1.05 | R_VTA | midbrain | 1.02 |
| | R_Hypothalamus_Medial | limbic system | 1.08 | L_Substantia_Innominata | medial temporal lobe | 1.04 |
| | L_Raphe | midbrain | 1.10 | L_Olfactory_Tubercle | medial temporal lobe | 1.04 |
| | R_Hippocampus_Postero_Dorsal | limbic system | 1.12 | R_IPAC | subcortical regions | 1.16 |
| | R_IPAC | subcortical regions | 1.16 | R_Hippocampus_Postero_Dorsal | limbic system | 1.17 |
| | R_Thalamus_Dorsolateral | subcortical regions | 1.16 | R_Cortex_Entorhinal | limbic system | 1.23 |
| | L_Substantia_Nigra | midbrain | 1.18 | R_Hippocampus_Posterior | limbic system | 1.29 |
| | R_Hippocampus_Ventral | limbic system | 1.19 | R_Hypothalamus_Medial | limbic system | 1.48 |
| | R_Hypothalamus_Lateral | limbic system | 1.32 | L_Hypothalamus_Medial | limbic system | 1.61 |
| | L_Hypothalamus_Lateral | limbic system | 1.40 | L_Ventral_Pallidum | subcortical regions | 1.78 |
| | L_Hypothalamus_Medial | limbic system | 1.46 | R_Substantia_Nigra | midbrain | 1.90 |
| | R_Hippocampus_Subiculum | limbic system | 1.60 | L_AcbSh | limbic system | 1.95 |
| | R_AcbSh | limbic system | 1.63 | R_AcbSh | limbic system | 1.97 |
| | R_Cortex_Motor | parietal lobes | 1.66 | R_CortexPiriform | limbic system | 2.10 |
| | L_Diagonal_Band | medial temporal lobe | 1.66 | L_HypothalamusLateral | limbic system | 2.14 |
| | R_Diagonal_Band | medial temporal lobe | 1.76 | R_OlfactoryTubercle | medial temporal lobe | 2.25 |
| | L_OlfactoryTubercle | medial temporal lobe | 2.06 | L_CortexPiriform | limbic system | 2.28 |
| | L_VentralPallidum | subcortical regions | 2.22 | R_VentralPallidum | subcortical regions | 2.87 |
| | R_CortexPiriform | limbic system | 2.25 | | | |
| | R_VentralPallidum | subcortical regions | 2.33 | | | |
| | R_OlfactoryTubercle | medial temporal lobe | 2.99 | | | |
| | L_AccumbensShell | limbic system | 3.18 | | | |
| model | R_AcbSh | limbic system | 1.01 | L_Hippocampus_Ventral | limbic system | 1.03 |
| | L_Cortex_Motor | parietal lobes | 1.07 | L_Pons | midbrain | 1.10 |
| | L_VTA | midbrain | 1.08 | R_AcbSh | limbic system | 1.18 |
| | L_Cortex_Piriform | limbic system | 1.09 | L_Hippocampus_Antero_Dorsal | limbic system | 1.21 |
| | L_Hypothalamus_Medial | limbic system | 1.10 | L_Hypothalamus_Lateral | limbic system | 1.21 |
| | R_Hypothalamus_Medial | limbic system | 1.13 | L_Substantia_Innominata | medial temporal lobe | 1.23 |
| | R_Substantia_Innominata | medial temporal lobe | 1.19 | L_Substantia_Nigra | midbrain | 1.28 |
| | R_Cortex_Entorhinal | limbic system | 1.19 | L_Diagonal_Band | medial temporal lobe | 1.42 |
| | L_Superior_Colliculus | midbrain | 1.27 | L_Hippocampus_Posterior | limbic system | 1.48 |
| | R_Substantia_Nigra | midbrain | 1.29 | L_AcbSh | limbic system | 1.50 |
| | R_Mesencephalic_Region | midbrain | 1.43 | R_Substantia_Nigra | midbrain | 1.51 |
| | L_Hippocampus_Posterior | limbic system | 1.45 | L_Hypothalamus_Medial | limbic system | 1.52 |
| | L_Hippocampus_Subiculum | limbic system | 1.49 | R_Hippocampus_Posterior | limbic system | 1.55 |
| | R_Cortex_Piriform | limbic system | 1.50 | L_VTA | midbrain | 1.56 |
| | L_AcbSh | limbic system | 1.54 | R_VTA | midbrain | 1.77 |
| | L_Diagonal_Band | medial temporal lobe | 1.57 | R_Cortex_Piriform | limbic system | 1.88 |
| | R_Diagonal_Band | medial temporal lobe | 1.73 | L_Cortex_Piriform | limbic system | 1.90 |
| | L_Hypothalamus_Lateral | limbic system | 1.88 | L_Olfactory_Tubercle | medial temporal lobe | 2.15 |
| | R_Ventral_Pallidum | subcortical regions | 2.00 | R_Ventral_Pallidum | subcortical regions | 2.93 |
| | L_SubstantiaNigra | midbrain | 2.16 | L_Ventral_Pallidum | subcortical regions | 3.03 |
| | L_VentralPallidum | subcortical regions | 2.50 | R_Olfactory_Tubercle | medial temporal lobe | 3.21 |
| | R_OlfactoryTubercle | medial temporal lobe | 2.57 | | | |
| | L_OlfactoryTubercle | medial temporal lobe | 2.83 | | | |
| normal | R_AcbSh | limbic system | 1.01 | R_Diagonal_Band | subcortical regions | 1.01 |
| | L_Cortex_Motor | parietal lobes | 1.07 | L_Mesencephalic_Region | midbrain | 1.03 |
| | L_VTA | midbrain | 1.08 | L_Cortex_Entorhinal | limbic system | 1.05 |
| | L_Cortex_Piriform | limbic system | 1.09 | L_Hippocampus_Subiculum | limbic system | 1.14 |
| | L_Hypothalamus_Medial | limbic system | 1.10 | L_Hippocampus_Posterior | limbic system | 1.16 |
| | R_Hypothalamus_Medial | limbic system | 1.13 | L_Diagonal_Band | subcortical regions | 1.27 |
| | L_Cortex_Piriform | limbic system | 1.03 | R_Raphe | | 1.32 |

Table 1. Continued.

| group | hub regions | location | Multiple of SD | hub regions | location | Multiple of SD |
|---|---|---|---|---|---|---|
| | | | 1 month | | | 3 months |
| | R_Substantia_Innominata | medial temporal lobe | 1.05 | R_Hippocampus_Subiculum | limbic system | 1.35 |
| | R_AcbSh | limbic system | 1.05 | R_Hypothalamus_Medial | limbic system | 1.44 |
| | L_Raphe | midbrain | 1.08 | R_Olfactory_Nuclei | subcortical regions | 1.47 |
| | R_Cortex_Piriform | limbic system | 1.09 | L_Hypothalamus_Medial | limbic system | 1.47 |
| | R_ic | | 1.18 | R_AcbSh | limbic system | 1.51 |
| | L_AcbSh | limbic system | 1.22 | L_VTA | midbrain | 1.53 |
| | R_Hypothalamus_Medial | limbic system | 1.27 | L_AcbSh | limbic system | 1.70 |
| | L_Substantia_Nigra | midbrain | 1.33 | R_VTA | midbrain | 1.97 |
| | R_Amygdala | limbic system | 1.38 | L_Ventral_Pallidum | subcortical regions | 2.00 |
| | L_VTA | midbrain | 1.42 | L_Hypothalamus_Lateral | limbic system | 2.12 |
| | R_VTA | midbrain | 1.43 | R_Cortex_Piriform | limbic system | 2.29 |
| | L_Diagonal_Band | medial temporal lobe | 1.70 | L_Olfactory_Tubercle | medial temporal lobe | 2.35 |
| | R_Zona_Incerta | subcortical regions | 1.74 | R_Ventral_Pallidum | subcortical regions | 2.53 |
| | R_Raphe | midbrain | 1.82 | R_Olfactory_Tubercle | medial temporal lobe | 2.65 |
| | L_Olfactory_Tubercle | medial temporal lobe | 1.91 | L_Cortex_Piriform | limbic system | 3.08 |
| | R_Olfactory_Tubercle | medial temporal lobe | 1.99 | | | |
| | R_Hypothalamus_Lateral | limbic system | 2.07 | | | |
| | L_Hypothalamus_Medial | limbic system | 2.23 | | | |
| | R_Ventral_Pallidum | subcortical regions | 2.51 | | | |
| | L_Ventral_Pallidum | subcortical regions | 2.52 | | | |
| | L_Hippocampus_Subiculum | limbic system | 2.75 | | | |
| sham-EA | L_Globus_Pallidus | subcortical regions | 1.00 | R_Substantia_Innominata | medial temporal lobe | 1.01 |
| | L_Thalamus_Dorsolateral | | 1.02 | R_AcbC | limbic system | 1.24 |
| | L_Hippocampus_Postero_Dorsal | limbic system | 1.12 | L_Substantia_Nigra | midbrain | 1.24 |
| | R_Substantia_Innominata | medial temporal lobe | 1.25 | R_Hypothalamus_Medial | limbic system | 1.28 |
| | L_AcbSh | limbic system | 1.40 | R_Diagonal_Band | medial temporal lobe | 1.45 |
| | L_Hypothalamus_Medial | limbic system | 1.43 | R_Ventral_Pallidum | subcortical regions | 1.51 |
| | L_Pons | midbrain | 1.52 | R_Globus_Pallidus | subcortical regions | 1.61 |
| | R_Hypothalamus_Medial | limbic system | 1.57 | L_Hypothalamus_Lateral | limbic system | 1.66 |
| | L_Diagonal_Band | medial temporal lobe | 1.93 | L_Hypothalamus_Medial | limbic system | 1.68 |
| | R_Ventral_Pallidum | subcortical regions | 2.23 | L_Hippocampus_Postero_Dorsal | limbic system | 1.70 |
| | L_Cortex_Piriform | limbic system | 2.34 | L_Diagonal_Band | medial temporal lobe | 1.79 |
| | R_Cortex_Piriform | limbic system | 2.59 | L_AcbSh | | 1.80 |
| | R_Olfactory_Tubercle | medial temporal lobe | 2.65 | L_Olfactory_Tubercle | medial temporal lobe | 1.81 |
| | L_Olfactory_Tubercle | medial temporal lobe | 2.70 | R_Hypothalamus_Lateral | limbic system | 1.95 |
| | L_Ventral_Pallidum | subcortical regions | 3.05 | R_Cortex_Piriform | limbic system | 2.01 |
| | | | | L_Cortex_Piriform | limbic system | 2.09 |
| | | | | L_Substantia_Innominata | medial temporal lobe | 2.35 |
| | | | | R_Olfactory_Tubercle | medial temporal lobe | 2.52 |
| | | | | L_Ventral_Pallidum | subcortical regions | 3.35 |
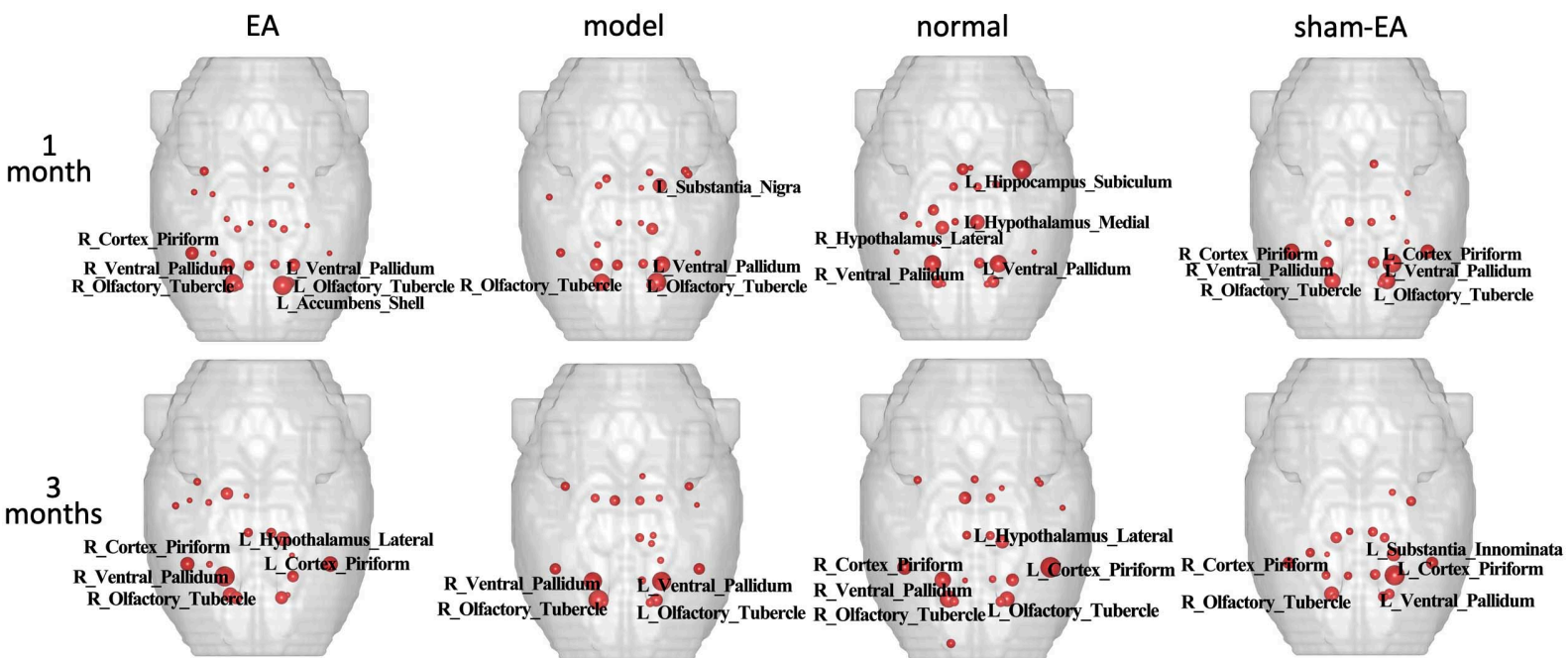
**Figure 3.** Hub regions of the functional neural networks of four groups of rats after one and three-months of intervention. More significant spheres show regions with a standard deviation higher than the average value of the nodal parameters.
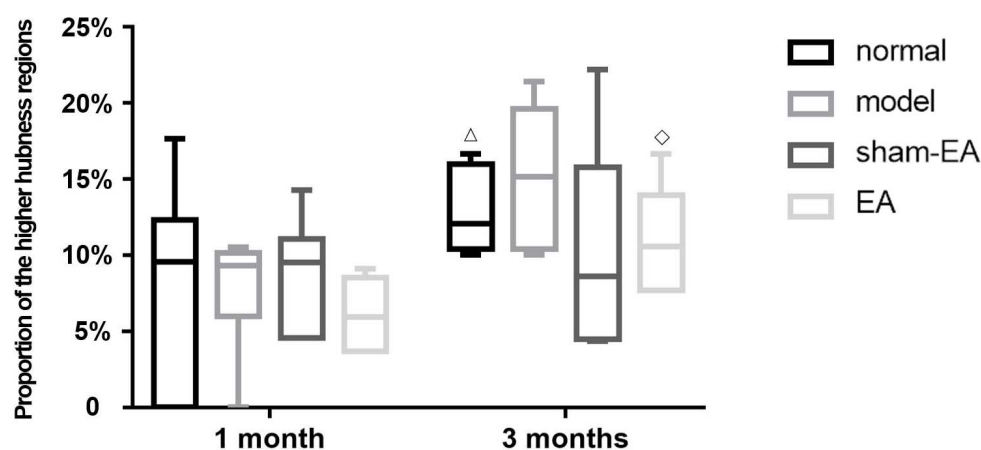


**Figure 4.** Differences in the proportion of more highly connected hub regions among four groups after one and three-months of intervention. △ $P < 0.05$, as compared to the normal group, ◊$P < 0.05$, as compared to the model group.

pothalamus and left amygdala exhibited significantly lower nodal properties in the EA group as compared to the sham-EA group. No significant difference was found among groups concerning degree.

## 4. Discussion

We presented the first longitudinal mapping study to explore the effect of EA on hub configurations associated with neuropathic pain. Apart from the significant pain-relief effect by EA, results exhibit differential alterations within the identified hub configurations. It was not the spatial distribution of hubs, but rather the hubness distribution that showed a significant difference among groups.

Previous studies have suggested that EA modulates the topological organization of whole-brain networks. However, subjects in previous studies were healthy individuals. Few studies have explored the effect of acupuncture on pathological conditions by application of a network analysis approach. Here, a rat model of neuropathic pain established by BPA allowed a comparison of nodal topological parameters and exploration of hub configurations of brain networks after EA intervention. Results showed that the spatial distribution of hub regions was similar among the four groups. For further analysis, hub regions were defined in each animal, and the proportion of more highly connected hub regions was compared among groups. A more substantial percentage of more highly connected hub regions were found in the model group

Table 2. Brain regions are showing significant differences in any of the three nodal properties.

| Brain regions | P -values | | |
| --- | --- | --- | --- |
| | Betweenness centrality | Degree | Nodal efficiency |
| after 1 month intervention | | | |
| EA vs. model | | | |
| EA > model none | | | |
| EA < model | | | |
| R_Mesencephalic_Region | - | 0.007 | - |
| L_Periaqueductal_Grey | - | 0.005 | - |
| model vs. normal | | | |
| model > normal | | | |
| R_Mesencephalic_Region | - | 0.003 | - |
| model < normal | none | | |
| EA vs. normal | | | |
| EA > normal | none | | |
| EA < normal | | | |
| L_Amygdala | 0.011 | - | - |
| EA vs. sham-EA | none | | |
| after 3 months of intervention | | | |
| EA vs. model | | | |
| EA > model | none | | |
| EA < model | | | |
| L_Hippocampus_Antero_Dorsal | 0.008 | - | - |
| model vs. normal | | | |
| model < normal | | | |
| R_Olfactory_Nuclei | 0.007 | - | - |
| model > normal | | | |
| L_Hippocampus_Antero_Dorsal | 0.011 | - | 0.002 |
| L_Pons | 0.001 | - | - |
| EA vs. normal | | | |
| EA > normal | none | | |
| EA < normal | | | |
| R_Olfactory_Nuclei | 0.005 | - | - |
| L_Amygdala | 0.004 | - | - |
| EA vs. sham-EA | | | |
| EA > sham-EA | none | | |
| EA < sham-EA | | | |
| R_Hypothalamus_Lateral | - | - | 0.001 |
| L_Amygdala | 0.009 | - | 0.002 |

than the normal group, while, after a three-month EA intervention, a smaller proportion was found in the EA group than the model group.

Neuropathic pain is a common symptom following nerve injury. Maladaptive central plasticity has been demonstrated to be involved in the development of neuropathological pain (Napadow et al., 2010; Naro et al., 2016), and Flor et al. (1995) used task-dependent fMRI to investigate brain changes of human patients following amputation. Their results showed that plastic changes occurred only in patients that experienced phantom limb pain but not in those without pain. Furthermore, the amount of cortical reorganization correlated positively with pain magnitude. Additionally, it was not only neuropathic pain associated with nociceptive processes but also with large-scale brain reorganization (Cauda et al., 2014). Mansour et al. (2016) investigated topological organizations of the human and rats brain connectome in three chronic pain conditions. Their findings suggested a state of global randomization of functional connectivity corresponded with chronic pain. Over the past few decades, plasticity has played a promising role in pain-relief therapies (Khu, 2015). Non-invasive brain stimulation techniques have been pursued as a therapeutic option in chronic pain via modulating activity in the target brain regions or a dysfunctional network (Naro et al., 2016). There has been clear evidence that these methods provide some pain relief by reverting maladaptive plasticity in neuropathic pain (Naro et al., 2016). Several studies have shown that EA promotion of functional neural recovery after nerve injury was dependent on the modulation of plastic changes associated with neurological diseases (He et al., 2014). In the present study, the result of BPA, changes characterized as a higher proportion of more highly connected hubs in the model group, suggests a type of maladaptive plasticity. Here it is proposed that, for the best functional outcome for pain relief, EA might restore an adaptive equilibrium to a disrupted network and suppress maladaptive plastic changes.

Additionally, nodal parameter changes showed a good match with the hub proportion distribution. At both time-points examined, nodal properties reflected a more highly connected network state, as evidenced by increased nodal efficiency, betweenness centrality and a degree in the model group when compared to the normal group, while these three nodal parameters exhibited decreases in the EA group when compared with the model group. Likewise, higher nodal parameter values in the model group were assumed to indicate a type of maladaptive plasticity, and EA is hypothesized to reverse the maladaptive, more highly connected state.

At the end of the first month of EA intervention, the right mesencephalic region exhibited a significantly higher degree in the model group than that in the normal group, while right mesencephalic region and left periaqueductal gray (PAG) showed a substantially lower degree in the EA group as compared to the model group. Mesencephalic region and PAG are the gray matter of a brainstem pain-modulation system, which is crucial for the maintenance of chronic pain (Mills et al., 2018). Brainstem activity in response to pain has commonly been reported as corresponding to PAG (Peyron et al., 2000). Further, the brainstem reticular formation has been demonstrated to be a vital component of the descending pain modulatory network. It has also been reported that

the mesencephalic reticular formation plays a crucial role in the development and maintenance of central sensitization and its clinical manifestation, secondary hyperalgesia (Zambreanu et al., 2005). Hyperalgesia in bilateral hindpaws resulting from BPA confirms from our research to be associated with a higher degree in the mesencephalic region when compared to a normal group and is considered to be maladaptive plastic change. One possible explanation for the lower degree centrality in the mesencephalic and periaqueductal gray in the EA group as compared to the model group is that EA might reverse the more highly connected maladaptive state of pain-related regions following neuropathic pain.

After a three-month EA intervention, nodal properties in hippocampal regions were significantly different across groups. Many studies evaluating the efficacy of acupuncture with neuroimaging tend to concentrate on brain regions within the pain matrix, associated with acute pain. Transition to chronic pain is associated with increased attention to pain, emotional rumination, nociceptive memory, and avoidance learning (Egorova et al., 2015). Pain and depression have been revealed to be clinically inter-related. It was reported that more than 50% of depressed patients suffered chronic pain, and the prevalence of affective diseases increases with the number of chronic pain sites (Annagür et al., 2014; Nicholl et al., 2014). Hippocampus, regions of the default mode network, were found to show functional alterations in patients and animal models of depression and chronic pain (Bilbao et al., 2018; Posner et al., 2016; Sambataro et al., 2014; Wise et al., 2016).

Additionally, the previous study has revealed that the functionally integrated areas of brachial plexus pain processing involve the entorhinal-hippocampus pathway, which is part of the Papez circuit (Wang et al., 2019). This has confirmed the involvement of cognitive function in plasticity changes after brachial plexus pain. In this context, it has been proposed that the higher nodal properties of the hippocampus in the model group compared with the normal group might be due to the link between depression and/or cognition and chronic pain. Results have also revealed that EA could reverse the higher nodal properties in hippocampal regions. However, possible interpretations are limited in the absence of any report on changes of depressive- and cognitive-like behavior.

## 5. Conclusion

A long-term EA intervention was performed in the rat on a clinically relevant neuropathic pain model induced by BPA. Nodal topological parameters and hub configurations of brain networks were investigated via a longitudinal graph theory study. Results showed that long-term EA could alleviate chronic neuropathic pain. fMRI data showed that pain-related changes might be associated with an increased proportion of more highly connected hub regions and increased nodal properties in hippocampal and mesencephalic regions and that these changes may be reversible through long-term EA intervention. It is proposed that EA might restore an adaptive equilibrium in a disrupted network and suppress maladaptive plastic changes associated with neuropathic pain. This explanation provides a potential mechanism for the pain relief effects of EA.

## Abbreviation

EA, electroacupuncture; BPA, brachial plexus avulsion; MWT, mechanical withdrawal threshold; EPI, echo-planar image; fMRI, functional magnetic resonance imaging; DICOM, Digital Imaging, and Communications in Medicine; NIFTI, Neuroimaging Informatics Technology Initiative; SD, standard deviation; FDR, false discovery rate; VTA, ventral tegmental area; ic, internal capsule; AcbSh, nucleus accumbens shell; AcbC, nucleus accumbens core; IPAC, Interstitial nucleus of the posterior limb of the anterior commissure; PAG, periaqueductal gray.

## Author contributions

X. H., M. Z., and J. X. conceived and designed the experiments; S. W. performed the experiments; J. W. and Y. L. analyzed the data; J. W. wrote the paper.

## Conflict of Interest

The authors declare no conflict of interest.

## References

Achard, S. and Bullmore, E. (2007) Efficiency and cost of economical brain functional networks. *PLoS Computational Biology* **3**, e17.

Annagür, B. B., Uguz, F., Apiliogullari, S., Kara, İ. and Gunduz, S. (2014) Psychiatric disorders and association with quality of sleep and quality of life in patients with chronic pain: A SCID-based study. *Pain Medicine* **15**, 772-781.

Bilbao, A., Falfán-Melgoza, C., Leixner, S., Becker, R., Singaravelu, S. K., Sack, M., Sartorius, A., Spanagel, R. and Weber-Fahr, W. (2018) Longitudinal structural and functional brain network alterations in a mouse model of neuropathic pain. *Neuroscience* **387**, 104-115.

Cauda, F., Palermo, S., Costa, T., Torta, R., Duca, S., Vercelli, U., Geminiani, G. and Torta, D. M. E. (2014) Gray matter alterations in chronic pain: A network-oriented meta-analytic approach. *NeuroImage Clinical* **4**, 676-686.

Chaplan, S. R., Bach, F. W., Pogrel, J. W., Chung, J. M. and Yaksh, T. L. (1994) Quantitative assessment of tactile allodynia in the rat paw. *Journal of Neuroscience Methods* **53**, 55-63.

Chen, H., Huang, M. and Yu, W. (2018) After effect of electroacupuncture at Jiaji acupoint on the protein expression of P2X4, P2X7 in chronic constriction injury rats. *Rehabilitation Medicine* **28**, 37-40. (In Chinese)

Chen, H., Liu, T. Y., Kuai, L., Zhu, J., Wu, C. J. and Liu, L. M. (2013) Electroacupuncture treatment for pancreatic cancer pain: a randomized controlled trial. *Pancreatology* **13**, 594-597.

Dhond, R. P., Kettner, N. and Napadow, V. (2007) Neuroimaging

acupuncture effects in the human brain. *Journal of Alternative and Complementary Medicine* **13**, 603-616.

Dhond, R. P., Yeh, C., Park, K., Kettner, N. and Napadow, V. (2008) Acupuncture modulates resting state connectivity in default and sensorimotor brain networks. *Pain* **136**, 407-418.

Egorova, N., Gollub, R. L. and Kong, J. (2015) Repeated verum but not placebo acupuncture normalizes connectivity in brain regions dysregulated in chronic pain. *NeuroImage Clinical* **9**, 430-435.

Fang, J., Jin, Z., Wang, Y., Li, K., Kong, J., Nixon, E. E., Zeng, Y., Ren, Y., Tong, H., Wang, Y., Wang, P. and Hui, K. K. (2009) The salient characteristics of the central effects of acupuncture needling: Limbic-paralimbic-neocortical network modulation. *Human Brain Mapping* **30**, 1196-1206.

Flor, H., Elbert, T., Knecht, S., Wienbruch, C., Pantev, C., Birbaumers, N., Larbig, W. and Taub, E. (1995) Phantom-limb pain as a perceptual correlate of cortical reorganization following arm amputation. *Nature* **375**, 482-484.

Fox, M. D., Zhang, D., Snyder, A. Z. and Raichle, M. E. (2009) The global signal and observed anticorrelated resting state brain networks. *Journal of Neurophysiology* **101**, 3270-3283.

Freeman, L. C. (1977) A set of measures of centrality based on betweenness. *Sociometry* **40**, 35.

Han, J. S. (2004) Acupuncture and endorphins. *Neuroscience Letter* **361**, 258-261.

He, X., Zhu, Y., Li, C., Park, K., Mohamed, A. Z., Wu, H., Xu, C., Zhang, W., Wang, L., Yang, J. and Qiu, B. (2014) Acupuncture-induced changes in functional connectivity of the primary somatosensory cortex varied with pathological stages of Bell's palsy. *NeuroReport* **25**, 1162-1168.

He, Y., Wang, J., Wang, L., Chen, Z. J., Yan, C., Yang, H., Tang, H., Zhu, C., Gong, Q., Zang, Y. and Evans, A. C. (2009) Uncovering intrinsic modular organization of spontaneous brain activity in humans. *PloS One* **4**, e5226.

Hui, K. K. S., Liu, J., Marina, O., Napadow, V., Haselgrove, C., Kwong, K. K., Kennedy, D. N. and Makris, N. (2005) The integrated response of the human cerebro-cerebellar and limbic systems to acupuncture stimulation at ST 36 as evidenced by fMRI. *NeuroImage* **27**, 479-496.

Khu, K. J. (2015) Neuroplasticity and brachial plexus injury. *World Neurosurgery* **84**, 1509-1510.

Liu, B., Chen, J., Wang, J., Liu, X., Duan, X., Shang, X., Long, Y., Chen, Z., Li, X., Huang, Y. and He, Y. (2012) Altered small-world efficiency of brain functional networks in acupuncture at ST36: A functional MRI study. *PLoS ONE* **7**, e39342.

Liu, L. A., Zhang, S., Wang, H. and Tang, L. X. (2016) Acupuncture combined with moxibustion plaster for nerve-root type cervical spondylosis. *Chinese Acupuncture & Moxibustion* **36**, 139-143. (In Chinese)

Luo, F. and Wang, J. Y. (2008) Modulation of central nociceptive coding by acupoint stimulation. *Neurochemical Research* **33**, 1950-1955.

Mansour, A., Baria, A. T., Tetreault, P., Vachon-Presseau, E., Chang, P. C., Huang, L., Apkarian, A. V. and Baliki, M. N. (2016) Global disruption of degree rank order: a hallmark of chronic pain. *Scientific Report* **6**, 34853.

Mills, E. P., Di Pietro, F., Alshelh, Z., Peck, C. C., Murray, G. M., Vickers, E. R. and Henderson, L. A. (2018) Brainstem pain-control circuitry connectivity in chronic neuropathic pain. *Journal of Neuroscience* **38**, 465-473.

Moya, J., Samper-Belda, F. J., Canals, S. and Moratal, D. (2015) Neurosurgery planning in rodents using a magnetic resonance imaging assisted framework to target experimentally defined networks. *Computer Methods and Programs in Biomedicine* **121**, 66-76.

Napadow, V., LaCount, L., Park, K., As-Sanie, S., Clauw, D. J. and Harris, R. E. (2010) Intrinsic brain connectivity in fibromyalgia is associated with chronic pain intensity. *Arthritis and Rheumatology* **62**, 2545-2555.

Naro, A., Milardi, D., Russo, M., Terranova, C., Rizzo, V., Cacciola, A., Marino, S., Calabro, R. S. and Quartarone, A. (2016) Non-invasive brain stimulation, a tool to revert maladaptive plasticity in neuropathic pain. *Frontiers in Human Neuroscience* **10**, 376.

Nicholl, B. I., Mackay, D., Cullen, B., Martin, D. J., Ul-Haq, Z., Mair, F. S., Evans, J., McIntosh, A. M., Gallagher, J., Roberts, B., Deary, I. J., Pell, J. P. and Smith, D. J. (2014) Chronic multisite pain in major depression

and bipolar disorder: cross-sectional study of 149,611 participants in UK Biobank. *BMC Psychiatry* **14**, 350.

Nijhuis, E. H. J., van Cappellen van Walsum, A. M. and Norris, D. G. (2013) Topographic hub maps of the human structural neocortical network. *PLoS ONE* **8**, e65511.

Peyron, R., Laurent, B. and García-Larrea, L. (2000) Functional imaging of brain responses to pain. A review and meta-analysis (2000). *Neurophysiologie Clinique-clinical Neurophysiology* **30**, 263-288.

Pomeranz, B. (1996) Scientific research into acupuncture for the relief of pain. *Journal of Alternative and Complementary Medicine* **2**, 53-60.

Posner, J., Cha, J., Wang, Z., Talati, A., Warner, V., Gerber, A., Peterson, B. S. and Weissman, M. (2016) Increased default mode network connectivity in individuals at high familial risk for depression. *Neuropsychopharmacology* **41**, 1759-1767.

Rodriguesfilho, R., Santos, A. R., Bertelli, J. A. and Calixto, J. B. (2003) Avulsion injury of the rat brachial plexus triggers hyperalgesia and allodynia in the hindpaws: a new model for the study of neuropathic pain. *Brain Research* **982**, 186-194.

Sambataro, F., Wolf, N. D., Pennuto, M., Vasic, N. and Wolf, R. C. (2014) Revisiting default mode network function in major depression: evidence for disrupted subsystem connectivity. *Psychological Medicine* **44**, 2041-2051.

Schwarz, A. J., Danckaert, A., Reese, T., Gozzi, A., Paxinos, G., Watson, C., MerloPich, E. V. and Bifone, A. (2006) A stereotaxic MRI template set for the rat brain with tissue class distribution maps and co-registered anatomical atlas: application to pharmacological MRI. *Neuroimage* **32**, 538-550.

Sporns, O. and Zwi, J. D. (2004) The small world of the cerebral cortex. *Neuroinformatics* **2**, 145-162.

Suo, X., Lei, D., Li, K., Chen, F., Li, F., Li, L., Huang, X., Lui, S., Li, L., Kemp, G. J. and Gong, Q. (2015) Disrupted brain network topology in pediatric posttraumatic stress disorder: A resting-state fMRI study. *Human Brain Mapping* **36**, 3677-3686.

Tian, L., Wang, J., Yan, C. and He, Y. (2011) Hemisphere- and gender-related differences in small-world brain networks: A resting-state functional MRI study. *NeuroImage* **54**, 191-202.

van den Heuvel, M. P. and Sporns, O. (2011) Rich-club organization of the human connectome. *Journal of Neuroscience* **31**, 15775-15786.

Wang, S., Ma, Z., Lu, Y., Wu, J., Hua, X., Zheng, M. and Xu, J. (2019) The localization research of brain plasticity changes after brachial plexus pain: sensory regions or cognitive regions? *Neural Plasticity* **2019**, 1-10.

Wang, J., Wang, X., Xia, M., Liao, X., Evans, A. and He, Y. (2015) GRETNA: a graph theoretical network analysis toolbox for imaging connectomics. *Frontiers in Human Neuroscience* **9**, 386.

Watts, D. J. and Strogatz, S. H. (1998) Collective dynamics of 'small-world' networks. *Nature* **393**, 440-442.

Wise, T., Radua, J., Via, E., Cardoner, N., Abe, O., Adams, T. M., Amico, F., Cheng, Y., Cole, J. H., de Azevedo Marques Périco, C., Dickstein, D. P., Farrow, T. F. D., Frodl, T., Wagner, G., Gotlib, I. H., Gruber, O., Ham, B. J., Job, D. E., Kempton, M. J., Kim, M. J., Koolschijn, P. C. M. P., Malhi, G. S., Mataix-Cols, D., McIntosh, A. M., Nugent, A. C., O'Brien, J. T., Pezzoli, S., Phillips, M. L., Sachdev, P. S., Salvadore, G., Selvaraj, S., Stanfield, A. C., Thomas, A. J., van Tol, M. J., van der Wee, N. J. A., Veltman, D. J., Young, A. H., Fu, C. H., Cleare, A. J. and Arnone, D. (2016) Common and distinct patterns of grey-matter volume alteration in major depression and bipolar disorder: evidence from voxel-based meta-analysis. *Molecular Psychiatry* **22**, 1455-1463.

Wu, J. J., Lu, Y. C., Hua, X. Y., Ma, S. J., Shan, C. L. and Xu, J. G. (2018) Cortical remodeling after electroacupuncture therapy in peripheral nerve repairing model. *Brain Research* **1690**, 61-73.

Xu, K. D., Liang, T., Wang, K. and Tian, D. A. (2010) Effect of pre-electroacupuncture on p38 and c-Fos expression in the spinal dorsal horn of rats suffering from visceral pain. *Chinese Medical Journal* **123**, 1176-1181.

Xu, P., Huang, R., Wang, J., Van Dam, N. T., Xie, T., Dong, Z., Chen, C., Gu, R., Zang, Y. F., He, Y., Fan, J. and Luo, Y. (2014) Different topological organization of human brain functional networks with eyes open versus eyes closed. *NeuroImage* **90**, 246-255.

Zambreanu, L., Wise, R. G., Brooks, J. C. W., Iannetti, G. D. and Tracey, I. (2005) A role for the brainstem in central sensitisation in humans. Evidence from functional magnetic resonance imaging. *Pain* **114**, 397-407.

Zhang, R., Lao, L., Ren, K. and Berman, B. M. (2014) Mechanisms of acupuncture-electroacupuncture on persistent pain. *Anesthesiology* **120**, 482-503.